Available online at www.sciencedirect.com

SciVerse ScienceDirect

Ceramics International 39 (2013) 7135–7142

CERAMICS INTERNATIONAL

www.elsevier.com/locate/ceramint

Degradation behavior of 4D carbon/carbon composites under supersonic oxidative air plasma

Shameel Farhan[a], Noaman Ul-Haq[a,*], Wen-Shyong Kuo[b]

[a]School of Chemical and Materials Engineering (SCME), National University of Sciences and Technology (NUST), H-12, Islamabad, Pakistan
[b]Composite Laboratory, Department of Aerospace and Systems Engineering, Feng Chia University, Taiwan, ROC

Received 27 January 2013; accepted 18 February 2013
Available online 26 February 2013

Abstract

Four-directional (4D) carbon/carbon (C/C) composites were prepared using an intermediate modulus carbon fiber as the reinforcement and two kinds of coal tar pitches as the source for carbon matrix. After repeated high-pressure impregnation, carbonization and graphitization at 2250 °C, a high density of 1.86 g/cm^3 was achieved. A plasma arc jet was applied to the composite for studying its degradation behavior. The oxidative supersonic jet was generated by an air plasma torch. For studying various stages of degradation during a long exposure time of 90-s, the intermittent ablation and erosion rates were measured for the C/C composite at time intervals of 70, 50 and 30 s. The mass ablation rate was increased rapidly with the time, while the erosion showed a bilinear response with a decreasing trend. The results were discussed based on the machined and eroded surfaces of the test samples. For studying the residual ablative performance, the samples of 30–70 s were then re-ablated and re-eroded in steps of 20-s so that all the samples are equal in total exposure time. The samples showed decreasing trends in the re-ablation and re-erosion rates and ultimately became zero for the last 20-s exposure time. There was a progressive increase in the char layer on the samples with the re-ablation. The porous char layer protected the samples against chemical and mechanical actions of the plasma stream. Compressive tests were carried out, and the decrease in the modulus was due to the presence of microcracks resulting from the mismatch in thermal expansion of the fiber and the matrix. The SEM micrographs reveal that inter- and intra-bundle cracks tend to grow through the weaker matrix pockets.

Keywords: A. Hot isostatic pressing; B. Composites; C. Ablation; E. Thermal applications

1. Introduction

Carbon/carbon (C/C) composites are unique materials from the standpoint of their thermal and mechanical properties. The properties such as low density, low coefficient of thermal expansion (CTE), high temperature stability, high thermal conductivity, and high strength and stiffness make C/C composites ideal for specific aerospace and commercial applications [1]. At temperatures above 1000 °C, the specific strength exceeds that of both ceramics and super alloys. In fact, the strength and stiffness increase with the temperature up to 2200 °C due to improved coupling between the fiber and matrix [2]. C/C composites were originally used on ablative structures (e.g., rocket nozzles, re-entry nose tips and leading edges) in which the materials have to endure high thermal gradients and complex mechanical stresses. However, more applications are found in high-speed braking systems for aircrafts, trains, and racing cars [3–6]. The material studied in this research is three-dimensional and four-directional (4D) in structure. The 4D C/C composites are well known for their excellent thermophysical and thermomechanical properties in short-term, high-temperature applications [7–10]. The fibrous preform is the structural backbone of the composite. The 4D structures approach isotropy in construction, and they are ideal for high-temperature and high-stress applications [11]. Due to the high interlaminar shear strength, they exhibit high performance, high shape stability and low erosion [12]. They are highly damage-tolerant at elevated temperatures under hostile conditions [12]. Many experimental characterizations of C/C composites have been reported in literature [13–15]. The oxyacetylene flame ablation and

*Corresponding author. Tel.: +92 51 90855106.
E-mail address: noaman@scme.nust.edu.pk (N. Ul-Haq).

0272-8842/$ - see front matter © 2013 Elsevier Ltd and Techna Group S.r.l. All rights reserved.
http://dx.doi.org/10.1016/j.ceramint.2013.02.056

plasma arc ablation are the most widely used methods to study the ablation behavior of C/C composites [16–20]. The experiments include micro, meso and macroscopic observations of the ablated surface and the measurements of the recession rate. The ablated surface morphology generally consists of fiber denudation and block denudation, while the recession rates can be expressed in terms of the linear erosion rate and the mass ablation rate. The effect of different exposure times in a plasma jet on the degradation behavior and re-ablation and re-erosion behavior has not been reported in detail in open literature. Tang et al. [21] studied the ablation rate of C/C and the ultra-high temperature ceramics with time in oxyacetylene torch environment. Chen et al. [22] studied the ablation and erosion rates of C/C composites with the C–SiC–TaC multi-interlayer as a function of ablation time. Petraconi et al. [23] studied the specific mass loss as a function of exposure time for graphite and C/C composites in a high-enthalpy plasma jet. This paper focuses on the influence of different exposure times on ablation and erosion behavior of 4D C/C composites with similar thermo-physical properties. The rates thus obtained were plotted with time and the degradation trends were discussed. Variation in degradation trends was correlated with the machined surface of the specimen and the physical phenomena observed during testing. The specimens with short exposure time were further tested in multiple re-ablation experiments. For multiple re-ablation experiments, 20-s exposure time was selected. The tests were repeated until the change became negligible. Highly dense 4D C/C composites were prepared by infiltrating liquid pitch into the carbon fiber preform. A plasma arc jet generated by an air plasma torch was applied to the composite, and the linear erosion and mass ablation rates were measured. To further investigate the residual mechanical properties, the samples were tested for compression behavior and the tests were named as compression after ablation (CAA) after the name of famous test compression after impact (CAI).

2. Experimental procedure

2.1. Composite preparation

The intermediate modulus carbon fiber named IM7 (12k filament tow, 5570 MPa ultimate tensile strength, and 5.2 μm in diameter) was used as the reinforcement and coal tar pitch as the source for the carbon matrix. Three tows (12k × 3) of the fiber were combined and passed through a 15% polyvinyl alcohol (PVA) solution in a pultrusion machine. The excessive PVA was squeezed by passing through a series of carbide nozzles and the coated rods were dried in the box type heating ovens. The maximum fiber preheating and the rod post-treatment temperatures were 300 °C and 280 °C, respectively. The diameter of the stiffened carbon fiber rod was 1.18–1.19 mm. The PVA is an auxiliary material used for binding fibers together and it produces minimum coke residue (3–5%) after carbonization [24]. Two perforated plates were used for the weaving of 4D preform, one for holding the vertical rods and another for pressing the horizontal layers of the rods. Initially, steel wires were inserted vertically in the plate as *Z*-direction rods and the carbon rods were inserted at 0° in the XY plane. After rod insertion, the upper plate was moved down to press the last inserted layer. The plates were then rotated by 60°. By this way, the carbon fiber rods were placed in three directions in XY plane i.e. 0°, +60° and −60°. Finally, the 4th direction metallic rods were replaced with carbon fiber rods. Fig. 1 shows the as-received 4D composite and the schematic arrangement of rods in four directions. The preform was 200 mm in diameter and 250 mm in height. The preform possesses open porosity, and close pores are practically nonexistent. This is a feature critical to the later multiple impregnations of the liquid pitch [25]. The properties of the pitches used for densification are shown in Table 1.

The densification involved two preliminary cycles of pressure impregnation and carbonization (PIC) at 1.0 MPa using the type-A pitch following graphitization treatment at 2250 °C. The preliminary cycles were used to make the preform rigid. The type-A pitch with a low softening point can efficiently impregnate the preform at 1.0 MPa [26]. After these two cycles, the volumetric density of the preform was increased up to 1.15 g/cm^3. The perforated holding container was used to enhance the density at this stage. In order to open the paths for next impregnation and densification, the outer surfaces of the sample were machined. To conduct the high-pressure impregnation and carbonization cycles, the sample was placed in a steel container and the hot pitch was poured under vacuum. The mold was welded and the sample was carbonized at 750 °C under 750-bar pressure. This process was repeated four times with intermediate heat treatment at 2100 °C for pore opening, graphitization and strength enhancement [21]. The high-temperature (type-B) pitch was used for these densification stages. The pressure is the key factor that controls impregnation and carbonization [27]. After the final heat treatment at 1500 °C, the sample density, as measured by the Archimedes method using Metller Toledo AG204 densitometer, was 1.86 g/cm^3.

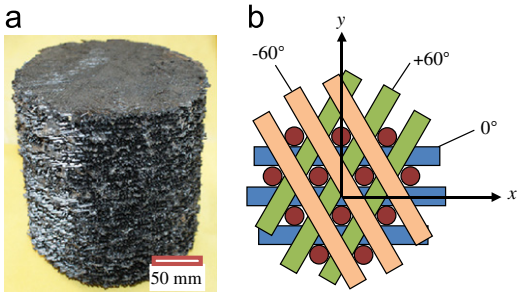

Fig. 1. Presentation of 4D preform: (a) a pictorial view and (b) schematic of the 4D structure and the arrangement of rods in the XY-plane.

2.2. Electric arc plasma testing

The electric arc plasma testing was conducted using a Huels type heater. The specimens are $75 \times 60\ mm^2$ in size and 13 mm in thickness, and they were exposed parallel to the plasma stream. The parallel configuration was adopted for simulating the high temperature conditions of a solid rocket motor nozzle where the hot combustion gases pass the throat axes. Air was heated by electrical discharge between the anode and the cathode in a water-cooled constrictor arc column. The heated air was supersonically expanded through a converging–diverging (test chamber) configuration. The parameters in the arc jet testing were Mach number 1.13–1.19, bulk enthalpy 3.3–3.5 MJ/kg, cold wall heat flux 4 MW/m^2, and the maximum temperature 2900–3000 °C. The ablation rates include the mass ablation rate and the linear erosion rate. The mass ablation rate is defined as the mass loss per unit time, while the linear erosion rate is the thickness reduction per unit time. Two tests were conducted for each duration of exposure time and the results were averaged. For the first set of tests, 90 s duration was selected based on maximum safe exposure time in the test bed. The specimen was named C90. To investigate the degradation profile for a total of 90-s, similar properties 4D C/C specimen were tested for 70, 50, and 30 s and named C70, C50 and C30, respectively. In order to investigate the residual ablation resistance, the C30, C50, and C70 samples were further subjected to re-ablation up to a total of 90-s. Each re-ablation time was set for 20-s. The C30 after three-times re-ablation is denoted as $C30(20)_3$. In the same manner, the samples C50 and C70 were also re-ablated two-times and one-time, respectively; they are denoted as $C50(20)_2$ and $C70(20)_1$, respectively. The morphology of the specimen after the plasma test was observed by the JEOL JSM 5910 scanning electron microscopy (SEM).

2.3. Compression after ablation (CAA)

The compression after ablation (CAA) of the material was studied using the SANS CMT 5105 (100 KN) mechanical testing machine. The vertical moving speed of the crosshead was set at 0.5 mm/min (corresponding to a strain rate of $5.5 \times 10^{-4}\ s^{-1}$) with the load and displacement being recorded. Based on Japanese Industrial Standard (JIS) R 7212, the specimens were cut to a cross-section of approximately $10 \times 10\ mm^2$ and a nominal length of 12.5 ± 0.3 mm (variation in height due to plasma erosion). Care was taken to avoid fraying and misalignment of fibers while preparing the specimens. The specimens were cut from the central portion of the plate where the ablation effect was the maximum. To create a smooth surface, a thin layer of ablated surface was removed by hand abrading using 300 grit SiC paper. The specimens were washed and dried in a drying oven at 110 °C for 120 min before the compressive tests.

3. Results and discussion

3.1. Erosion and ablation

Two sets of four arc jet tests were conducted, and the results are plotted in Fig. 2. For a duration of 90-s, the specimens

Table 1
Properties of pitches used for the processing of 4D C/C composite.

Pitch type	Softening point (°C)	Density (g/cm^3)	Carbon contents (%)	Hydrogen contents (%)	Solubility in toluene (%)	Coke yield (%)
Type A	65–70	1.21	90	5.2	68–75	37–40
Type B	135–145	1.30	93	4.5	25–55	52–62

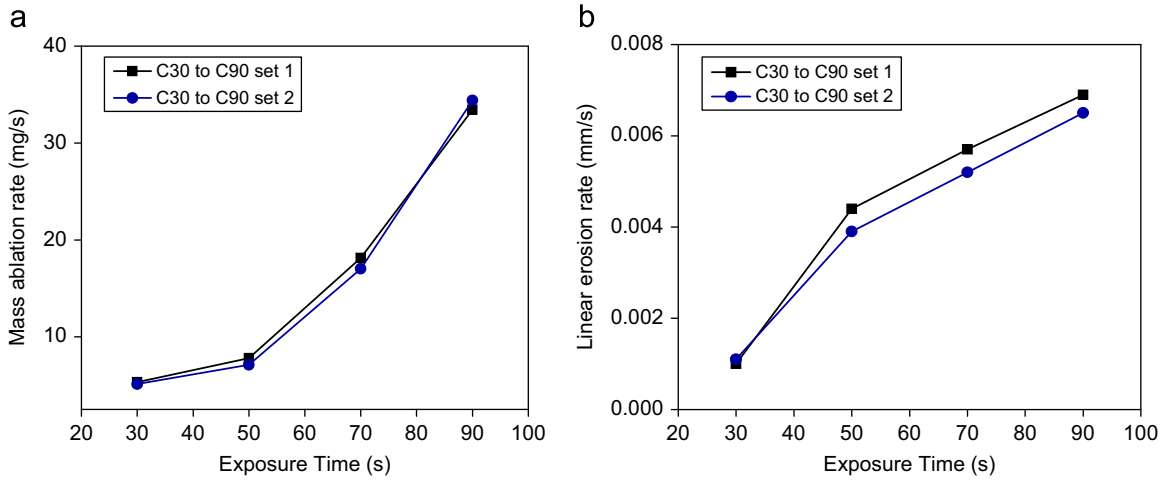

Fig. 2. Degradation behavior of 4D C/C composites: (a) mass ablation rate and (b) linear erosion rate.

showed an average mass ablation and linear erosion rates of 33.93 mg/s and 0.0067 mm/s, respectively. For degradation profile, the results of C70, C50, and C30 are shown in Table 2. Both the linear erosion and mass ablation rates are increased with the exposure time. The mass ablation rate is increased more pronouncedly with time, while the linear erosion shows a bilinear response with a decreasing trend. The mass ablation rate is generally considered to depend on the surface temperature of the composite. With the increase in exposure time, the surface temperature exceeded 2000 °C and mass loss increased rapidly. During the course of experiments, the degradation proceeded with a flaking action. White glowing particles discharged and observed visually moving along and scattering from the plasma stream. This is because of the presence of fiber debris resulting from the specimen machining. The machining also caused damage on fiber surface and fiber/matrix interface. The specimens were machined so that the XY plane carbon fiber rods were parallel to their rectangular face. Thickness of one layer of carbon fiber rods in XY plane is equal to diameter of a single pultruded rod, which is 1.18 mm in this case. After machining and grinding of the specimens, the surface was examined for straightness of carbon fibers. It was found that, in all the specimens, the upper most carbon rods layer was only 0.4 mm in thickness (Fig. 3) and the 0.78 mm was cut in machining. It is a random outcome in final machining and observed for these experiments. This 0.4 mm layer was parallel to the plasma flow. These fibers and surrounding matrix were removed at a faster rate due to strong shearing force of the flowing plasma stream.

Table 2
Individual and cumulative ablation and erosion rates of the samples.

Sample #	Exposure time (s)	Re-exposure time (s)	Mass ablation rate (mg/s)	Linear erosion rate (mm/s)
$C30(20)_3$	30	–	5.33	0.0010
		20	1.0	0.0005
		20	1.0	0.0005
		20	0.0	0.0000
$C50(20)_2$	50	–	19.40	0.0044
		20	1.0	0.0010
		20	0.0	0.0000
$C70(20)_1$	70	–	27.29	0.0057
		20	1.0	0.0005
C90	90	–	33.93	0.0067

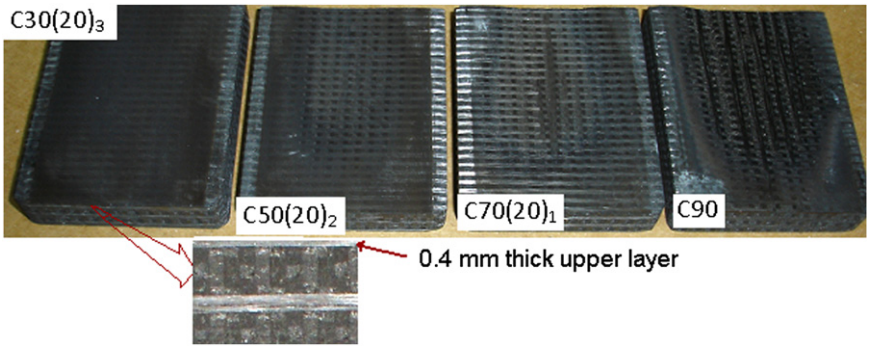

Fig. 3. Ablation morphologies of all the samples.

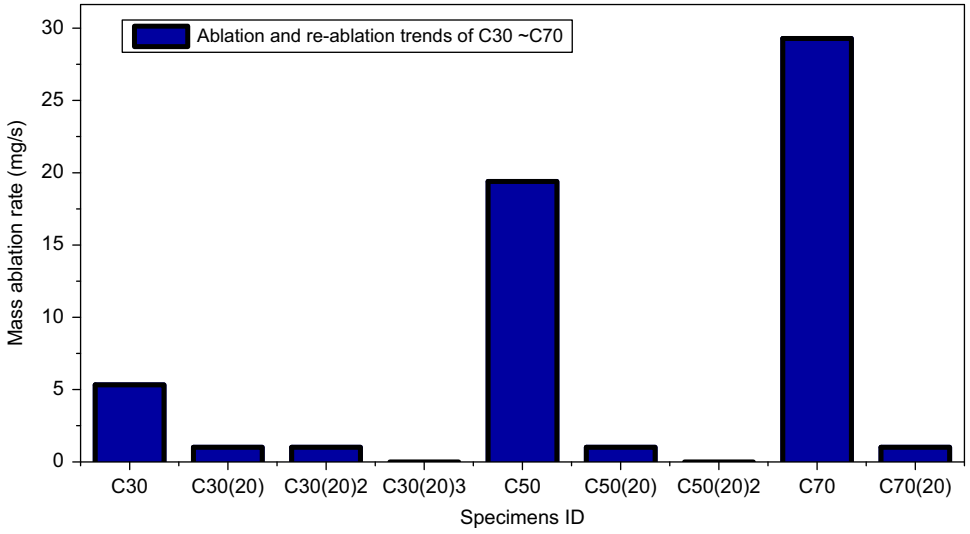

Fig. 4. Mass ablation and re-ablation trends of C30–C70 specimens.

These chunks of fibers and matrix were seen as white glowing particles between the 20th and 45th second of the exposure time. Once these fibers and matrix were removed, the linear erosion rate slowed down. Initial higher linear erosion rate resulting from removal of short cut fibers and matrix, also controlled the rise in temperature of specimens and hence lower mass ablation rate for short duration of exposure time. Once these particles removed, the specimen temperature started rising at a faster rate resulting in a higher mass loss due to oxidation for long exposure time. This phenomenon is evident in the macroimages of the ablated specimens (Fig. 3). The upper 0.4 mm (about one-third of the layer) of the carbon rod layer is visible in the sample $C30(20)_3$ after 30-s ablation and 20-s re-ablation tests. The upper 0.4 mm layer became thinner in $C50(20)_2$, partially removed in C70(20) and completely removed in the sample C90 (0.6 mm linear erosion in 90-s). For residual ablative properties, the results of re-ablation of C30–C70 are summarized in Table 2. The ablated sample C30 showed progressive decrease in erosion and ablation rates and finally showed zero rates when exposed to the 4th time of 20-s test. The samples C50 and C70 also showed the same decreasing trend and the results are plotted in Fig. 4. It is to be noted that all the specimens in re-ablation test showed a mass ablation and linear erosion rate of 1.0 mg/s and 0.0005 mm/s, respectively. The sample C30 was fully covered with a char layer that was sticky and black in color.

Table 3
Average compressive strength and modulus of the degraded samples.

Sample ♯	Exposure time (s)	Re-exposure time (s)	Ultimate compressive strength (MPa)	Compressive modulus (GPa)
$C30(20)_3$	30	20+20+20	84	8.0
$C50(20)_2$	50	20+20	83	8.0
$C70(20)_1$	70	20	83	5.0
C90	90	–	76	4.5

There was a progressive decrease in char deposit from the sample C30 to C90. The flowing gaseous products introduced too much carbon at these temperatures. As a result, a solid carbon deposit was formed in the sample C30, and it can reduce the porosity and the permeability, and increase the local density [28,29]. This effect increased the resistance to the thermo-chemical ablation. The sample C30 showed an ablation rate of 5.33 mg/s for the first 30-s ablation. The rate is reduced to 1.0 mg/s in the second and third re-ablation tests due to the insulation effect of the thickened char layer. The sample showed no further change for the last 20-s ablation. The char layer also progressively increased as shown in Fig. 3. For a longer duration of plasma exposure, such as the sample C90, the temperature just below the exposed surface reached in the range of 2500 °C–2800 °C. The thermodynamic conditions and the chemical species available in the internal gas flow changed the direction of gas/solid reactions. Therefore, instead of being deposited as the char layer, the carbon of the residue was turned into gaseous species, and as a result, the mass loss is increased [24,25]. Moreover, due to the long ablation and erosion time, the char layer (if produced) was also constantly removed because of the high shear force caused by the plasma flow.

3.2. Compressive behavior

Table 3 shows the average residual compressive strength and modulus. The load–displacement curves of the specimens are shown in Fig. 5. The linear region, representing the true elastic response of the material was used to calculate the compressive modulus. The peak portion between 0.2 and 0.4 mm displacement is the ultimate compressive load. The compressive strength of all the samples except C90 was almost the same. The modulus started decreasing for the samples C70 and C90. The sample C90 showed the lowest residual strength and modulus. This sample was exposed in plasma stream for the longest exposure time of

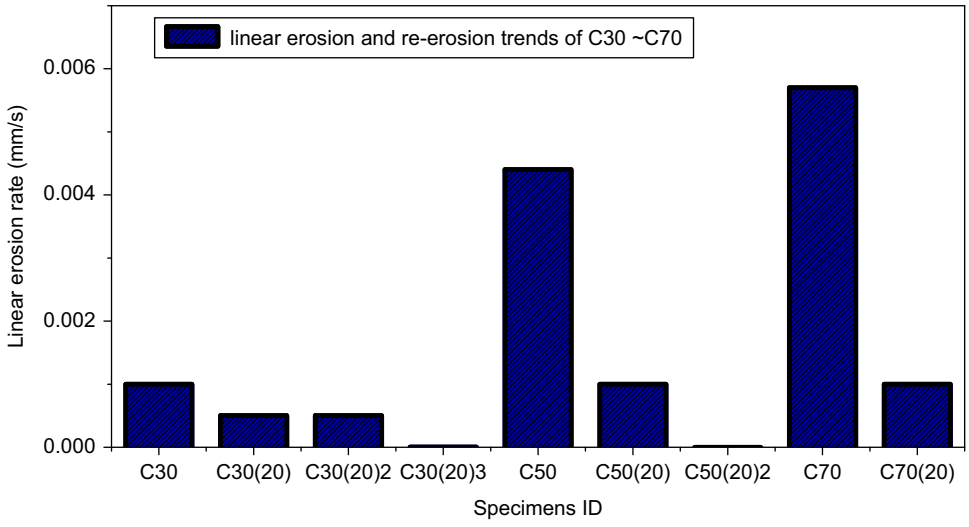

Fig. 5. Linear erosion and re-erosion trends of C30–C70 specimens.

90-s, resulting in deep penetration into the interfacial areas of the composite. The temperature of the flowing plasma stream was 3000 °C with a Mach number of 1.19. The sample C90 experienced the highest temperature for the longest time interval. After 90-s, the plasma flow was stopped and the sample cooled down at a very fast rate. The fiber and the matrix, with different CTEs, were experienced uneven expansions and contractions, resulting in micro-cracks in the matrix and interface. The modulus therefore decreased from 4.5 GPa. Although the load–displacement curves show typical brittle behavior, with a rapid decline, the material did not undergo a catastrophic failure. All the samples show end crushing (Fig. 6) at the plasma-affected face due to buckling of carbon rods and matrix crushing. The plots for the sample C90 demonstrate large variation in linear portion and a lower modulus. The presence of surface cracks affects the modulus and strength [30]. The surface of the sample C90 was the most degraded and was less tough than the baseline material. The 3D C/C composites show extremely low interfacial strength between the fiber and the matrix [31]. The end crushing was due to the weak interfacial strength in the plasma-affected areas. When the compressive load was applied on the specimen ends, shear stress is induced along the interface between specimen ends and loading plates [32]. The end crushing is also typical in block compression test methods. Fig. 7 shows the SEM micrographs of the sample $C30(20)_3$ and C90. The sample $C30(20)_3$ showed the lowest level of degradation, and the ablated surface

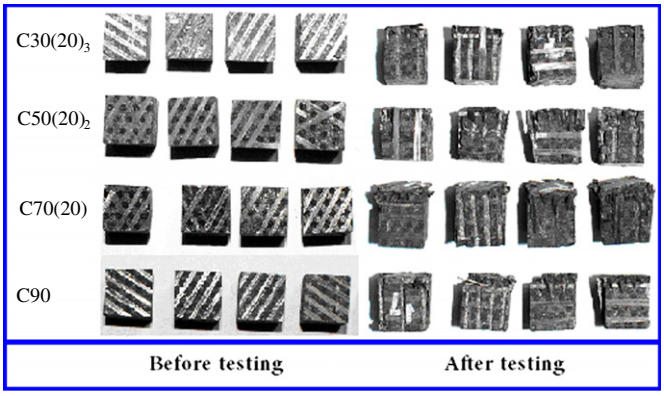

Fig. 7. Samples before and after compression testing.

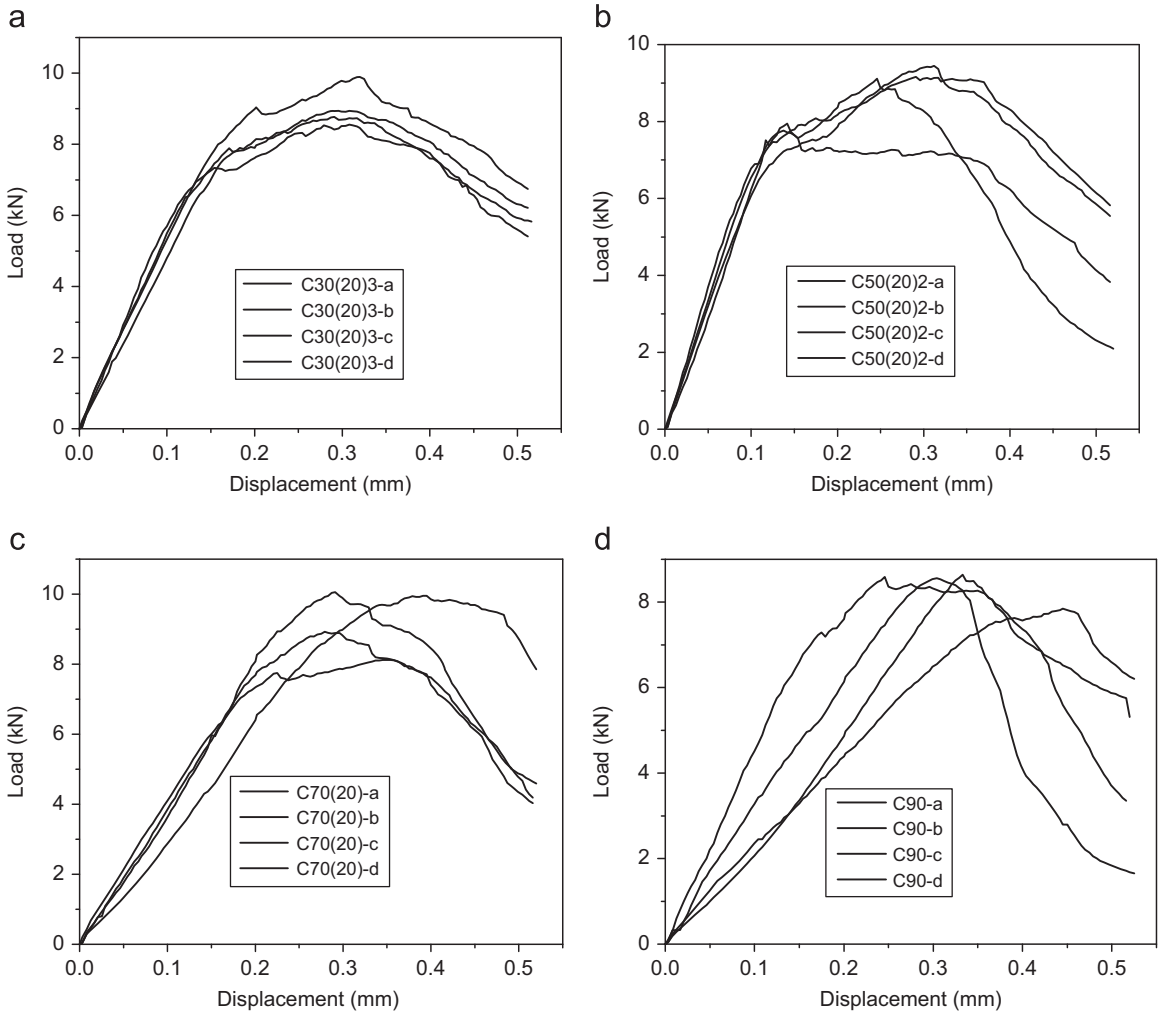

Fig. 6. Load–displacement curves of the samples: (a) $C30(20)_3$, (b) $C50(20)_2$, (c) C70(20) and (d) C90.

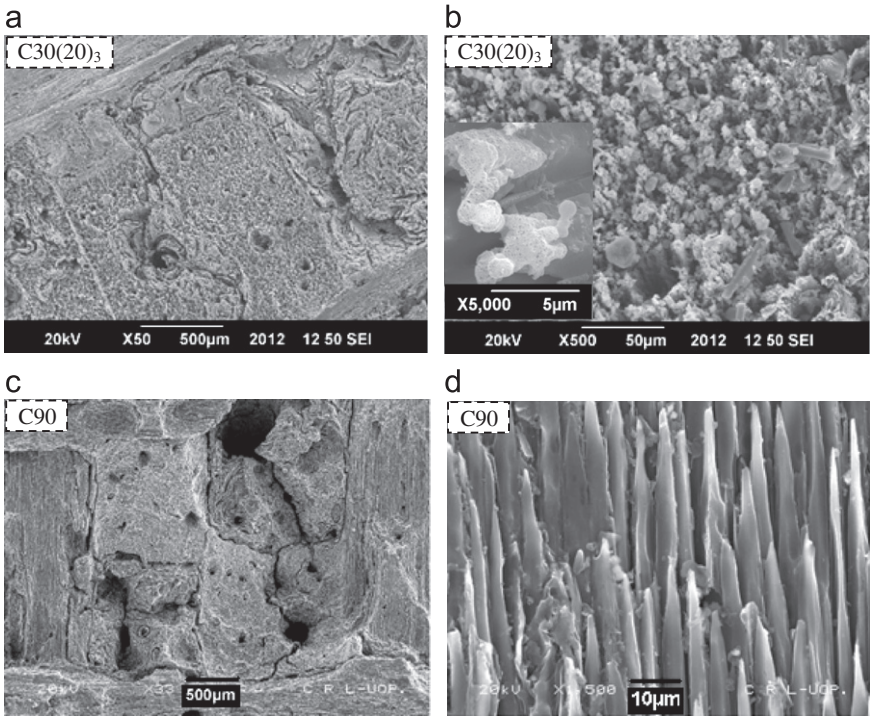

Fig. 8. Micrographs of the degraded samples: (a) $C30(20)_3$ and (b) C90.

was fully covered with porous char layer. It is clear in the inset SEM picture of the sample $C30(20)_3$ that the fiber tips acquired the shape of needle and covered with a porous char layer. In C90, due to a very high thermal-gradient with the surrounding temperature, some inter- and intra-bundle micro-cracks were created, and they can extend through the matrix pockets. The fibers parallel to the plasma flow became thinner and ultimately sharpened at the ends. The erosion occurred from some structural defects on the outermost shell of the fiber, resulting in the fiber island bonded to the fiber bundle by the non-eroded matrix (Fig. 8).

4. Conclusions

The 4D C/C composites were prepared using an intermediate modulus carbon fiber as the reinforcement and the carbon matrix derived from the coal tar pitch through the process of the high-pressure impregnation and carbonization. In order to investigate the degradation stages of a long exposure time in plasma stream, similar properties C/C samples were tested for 30–90 s. The results showed that the mass ablation rate increased rapidly with the increase in exposure time while the linear erosion rate showed a bilinear response with a decreasing trend. According to the SEM observations, machined and eroded surfaces of the test samples are discussed. The sample machining can cause fiber fragmentation and weaken the fiber/matrix interface. The shear forces of the plasma stream removed the fiber fragments, resulting in a higher initial erosion rate. Once these were removed, the underlying long fibers were exposed which showed better resistance against plasma shear forces with a decreasing erosion rate. In residual ablative performance tests, all the specimens showed decreasing trends in re-ablation and re-erosion rates and ultimately became zero for the last 20-s exposure time. The thickness of the char layer increased with the increasing number of the re-recession experiments. The char layer protected the samples against chemical and mechanical actions of the plasma stream. The sample $C30(20)_3$ with the thickest char layer showed very low re-ablation and re-erosion rates. The compressive properties of the samples C30 and C50 showed no significant loss when compared with a virgin specimen. The modulus of C90 was the lowest due to the presence of microcracks resulting from thermal stresses. The SEM micrographs also show that inter- and intra-bundle cracks can extend through carbon matrix pockets.

References

[1] G. Savage, Carbon/Carbon Composites, Chapman & Hall, London, 1993, pp. 173–174.
[2] G.A. Rozak, Mechanical Behavior of Carbon–Carbon Composites, NASA Contractor Report #174767, (1984).
[3] L. Dagli, Y. Remond, Identification of the non-linear behavior a 4D carbon–carbon material designed for aeronautic application, Applied Composite Materials 9 (2002) 1–15.
[4] K.Z. Li, X.T. Shen, H.J. Li, S.Y. Zhang, T. Feng, L.L. Zhang, Ablation of the carbon/carbon composite nozzle-throats in a small solid rocket motor, Carbon 49 (2011) 1208–1215.
[5] X. Aubard, C. Cluzel, L. Guitard, P. Ladeveze, Modeling of the mechanical behavior of 4D carbon/carbon composite materials, Composite Science and Technology 58 (1998) 701–708.

[6] S. Farhan, K.Z. Li, L.J. Guo, A novel thermal gradient chemical vapor infiltration process for carbon–carbon composites, New Carbon Materials 22 (2007) 247–252.
[7] X. Aubard, C. Cluzel, L. Guitard, P. Ladeveze, Damage modeling of a 4D carbon/carbon composite for high temperature application, Ceramics International 26 (2000) 631–637.
[8] L. Delneste, B. Perez, An inelastic finite element model of 4D carbon–carbon composites, AIAA Journal 21 (1983) 1463–1475.
[9] P. Lamicq, Recent improvements in 4D carbon–carbon materials, AIAA Journal 77 (1977) 822–834.
[10] J. Lachaud, N. Bertrand, G.L. Vignoles, G. Bourget, F. Rebillat, P. Weisbecker, A theoretical/experimental approach to the intrinsic oxidation reactivities of C/C composites and of their components, Carbon 45 (2007) 2768–2776.
[11] Y.J. Lee, H.J. Joo, Investigation on ablation behavior of CFRC composites prepared at different pressure, Composites A 35 (2004) 1285–1290.
[12] R.Z. Li, Y.D. Li, J.M. Su, H. Cui, Z.A. Su, S.J. Zhou, Study of the properties of axial rod 4D woven C/C composite, Extended abstracts, Eurocarbon 98, Strasbourg, France: Science and Technology of Carbon, (1998).
[13] J.C. Han, X.D. He, S.Y. Du, Oxidation and ablation of 3D carbon–carbon composite at up to 3000 °C, Carbon 33 (1995) 473–478.
[14] N.S. Jacobson, D.M. Curry, Oxidation microstructure studies of reinforced carbon/carbon, Carbon 44 (2006) 1142–1150.
[15] B. Chen, L.T. Zhang, L.F. Cheng, X.G. Luan, Erosion resistance of needled carbon/carbon composites exposed to solid rocket motor plumes, Carbon 47 (2009) 1474–1479.
[16] D. Chou, B.I. Yoon, Microstructural interpretation of the effect of various matrices on the ablation properties of carbon fiber reinforced composites, Composite Science and Technology 61 (2001) 271–280.
[17] J. Yin, X. Xiong, H. Zhang, B. Huang, Microstructure and ablation performances of dual-matrix carbon/carbon composites, Carbon 44 (2006) 1690–1694.
[18] B. Yan, Z.F. Chen, J.X. Zhu, J.Z. Zhang, Y. Jiang, Effects of ablation at different regions in three-dimensional orthogonal C/SiC composites ablated by oxyacetylene torch at 1800 °C, Journal of Material Processing Technology 209 (2009) 3438–3443.
[19] S. Farhan, K.Z. Li, L.J. Guo, Q.M. Gao, F.T. Lan, Effect of density and fiber orientation on the ablation behavior of carbon–carbon composites, New Carbon Materials 25 (2010) 161–167.
[20] T. Ogasawara, T. Ishikawa, T. Yamada, R. Yokota, M. Itoh, Thermal response and ablation characteristics of carbon fiber reinforced composite with novel silicon containing polymer MSP, Journal of Composite Materials 36 (2002) 143–157.
[21] S. Tang, J. Deng, S. Wang, W. Liu, K. Yang, Ablation behavior of ultra-high temperature ceramics composites, Material Science and Engineering A 465 (2007) 1–7.
[22] Z. Chen, X. Siong, G. Li, Y. Wang, Ablation behaviors of carbon/carbon composites with C–SiC–TaC multi-interlayers, Applied Surface Science 255 (2009) 9217–9223.
[23] G. Petraconni, et al., Degradation of carbon-based materials under ablative conditions produced by a high enthalpy plasma jet, Journal of Aerospace Technology and Management 2 (2010) 33–40.
[24] W. Gilman, L. VanderHart, T. Kashiwagi, ACS symposium series 599, in: G.L. Nelson (Ed.), In Fire and Polymer, American Chemical Society, Washington, DC, 1995, p. 161.
[25] E. Fitzer, L.M. Manocha, Carbon reinforcements and carbon/carbon composites, Springer, 1998, pp. 90–92.
[26] I.S. Oh, K.I. Kim, J.K. Kim, K.W. Kim, H.J. Doo, Effects of pressure on the pore formation of carbon/carbon composites during carbonization, Journal of Materials Science 34 (1999) 4585–4595.
[27] M.M. Sotaudehnia, A.K. Soltani, A. Maghsouipour, F. Moztarzadeh, The effect of modification of matrix on densification efficiency of pitch based carbon composites, Journal of Coal Science and Engineering 16 (2010) 408–414.
[28] K. Kuo, S. Keswani, A comprehensive theoretical model for carbon–carbon composite nozzle recession, Combustion Science and Technology 42 (1986) 177–192.
[29] F.S. Milos, Y.K. Chen, Comprehensive model for multicomponent ablation thermochemistry, in: Proceedings of the 35th Aerospace Science Meeting and Exhibit, AIAA, Reno, NV, (1997).
[30] H.Y. Luo, S. Roy, H.B. Lu, Dynamic compressive behavior of unidirectional IM7/5250-4 laminate after thermal oxidation, Composite Science and Technology 72 (2012) 159–166.
[31] M.S. Aly-Hassan, H. Hatta, S. Wakayama, M. Watanabe, K. Miyagawa, Comparison of 2D and 3D carbon/carbon composites with respect to damage and fracture resistance, Carbon 41 (2003) 1069–1078.
[32] H. Hatta, K. Tanigguchi, Y. Kogo, Compressive strength of three-dimensionally reinforced carbon/carbon composites, Carbon 43 (2005) 351–358.